# A Transcutaneous Carbon Dioxide Monitor Based on Time-Domain Dual Lifetime Referencing

Tuna B. Tufan, Ulkuhan Guler

***Abstract*—The partial pressure of arterial carbon dioxide plays a critical role in assessing the acid-base and respiratory status of the human body. Typically, this measurement is invasive and can only be taken momentarily when an arterial blood sample is drawn. Transcutaneous monitoring is a noninvasive surrogate method that provides a continuous measure of arterial carbon dioxide. Unfortunately, current technology is limited to bedside instruments mainly used in intensive care units. We developed a first-of-its-kind wearable transcutaneous carbon dioxide monitor that utilizes a luminescence sensing film and a time-domain dual lifetime referencing method. Benchtop experiments confirmed the monitor's ability to accurately identify changes in the partial pressure of carbon dioxide within the clinically significant range. Compared to the luminescence intensity-based technique, the time-domain dual lifetime referencing method is less prone to measurement errors caused by changes in excitation strength, reducing the maximum error from ∼40% to ∼3% and resulting in more reliable readings. Additionally, we analyzed the sensing film by investigating its behavior under various confounding factors and its susceptibility to measurement drift. Finally, a human subject test demonstrated the effectiveness of the applied method in detecting even slight changes in transcutaneous carbon dioxide, as small as ∼0.7%, during hyperventilation. The prototype, which consumes 30.1 mW of power, is a wearable wristband with compact dimensions of 37 mm× 32 mm.**

## I. Introduction

The ability to monitor patients not only in the clinic but also during their daily activities at their homes enables significant benefits, including 1) monitoring patients over long periods without lengthy hospital visits, 2) administering timely interventions, 3) reducing the risk of re-admittance, and 4) saving resources such as time and money. In today's healthcare system, this emerging concept is called remote patient monitoring. Moving the monitoring capabilities out of the clinic is a transition facilitated by advancements in sensing, materials, electronics, and communication technologies. Thanks to these advancements, bulky bench-top monitoring devices have been transforming into miniaturized wearables with wireless connectivity, enabling patients to pursue their day-to-day lives while being monitored by healthcare providers in real time. Fig.1 illustrates the examples of this transition in carbon dioxide monitoring from invasive blood gas analyzers to noninvasive wearable devices.

There is a pressing need to keep up the advancements in wearable technologies for respiration monitoring with miniaturized and noninvasive wearables. Respiratory diseases such as chronic obstructive pulmonary disease (COPD) and asthma are among the prevalent diseases, affecting and causing the death of millions of people worldwide every year [1], [2]. These diseases severely impact respiratory efficiency, potentially resulting in respiratory and neurological complications such as blackout, seizures, and brain injury, particularly in preterm neonates [3], [4]. Therefore, having the ability to monitor respiratory parameters remotely and continuously will allow for the timely detection of complications' onset and, consequently, the treatment of these diseases.


Fig. 1. Evaluation of $CO_2$ monitors from invasive arterial blood gas analyzers to noninvasive wearable transcutaneous devices. Original figures from [6]–[8]

According to medical literature, there is a direct correlation between respiratory efficiency and the partial pressure of carbon dioxide and oxygen in arteries, also known as $PaCO_2$ and $PaO_2$ [3]. The most reliable way to measure $PaCO_2$ and $PaO_2$ – blood gases – is arterial blood gas (ABG) analysis. However, a noninvasive and direct alternative to ABG analysis exists in the form of transcutaneous blood gases, which can serve as a surrogate measure of blood gases [5]. In this paper, our focus will be on transcutaneous carbon dioxide.

The difussion of carbon dioxide ($CO_2$) through capillaries and epidermis results in the formation of partial pressure of $CO_2$ ($PCO_2$) on the surface of the human skin, known as partial pressure of transcutaneous $CO_2$ ($PtcCO_2$). $PtcCO_2$ strongly associated with $PaCO_2$, indicating a high correlation between the two measures [9]–[11]. Hence, $PtcCO_2$ monitoring is a reliable surrogate for gold standard ABG analysis [12]. Moreover, since $PtcCO_2$ can be measured noninvasively, it enables healthcare providers to continuously monitor fluctuations in $CO_2$ levels. Especially in neonatal intensive care units, where patients require delicate care, $PtcCO_2$ monitoring has become a preferred method for tracking $CO_2$ trends, replacing ABG analysis [3], [13].

Traditionally, $PtcCO_2$ is measured with electrodes developed by Severinghaus, that are sensitive to the potential of hydrogen (pH) and correlated with the logarithm of $PtcCO_2$ [14]. Initially designed with large electrodes, the sensor size has eventually shrunk with the transition to microelectrodes, fitting both the electrodes and electronics into a volume as small as 120 $mm^3$ [15], [16]. Despite the fact that these

This material is based upon work supported in part by the National Science Foundation (NSF) under Grant EECS-2143898. Corresponding author: Ulkuhan Guler: uguler@wpi.edu.

$PtcCO_2$ sensors are small enough to be worn on the skin, they are wired to a benchtop monitor limiting the patient's mobility. This benchtop monitor consists of post-processing electronics, a docking station, along with a gas bottle for sensor calibration, which is critical for the accuracy of readings. When unused, the sensor has to be kept in this docking station for calibration with a gas mixture of known $PCO_2$ to avoid measurement drift over time. The calibration is required every 12 hours [16].

Traditional electrode-based $PtcCO_2$ sensors cannot be transformed into wearable devices for remote monitoring of patients during their daily activities, as the benchtop monitor and the calibration unit are essential parts of their system. These sensors are more suitable for bedside clinical use. That being said, researchers investigated various sensing methods to develop solutions for wearable applications, such as the infrared (IR) absorption principle of $CO_2$ [17]–[19] and $CO_2$'s quenching effect on the emission of $CO_2$-sensitive luminescence film [20], [21]. The luminescent sensors proved to be suitable for wearable $PtcCO_2$ monitoring due to their small size [22], fast response time [23], and high sensitivity [24].

We presented the proof-of-concept time-domain dual lifetime referencing-based $PtcCO_2$ monitoring prototype in [25]. In this paper, we extend our earlier work by additionally presenting: 1) a thorough analysis of the application of the t-DLR method and the effects of the confounding factors, 2) a smaller and lower-power prototype that fits into a wearable wrist enclosure, 3) $CO_2$-sensitive luminescence sensor and device characterization, and 4) results from human subject tests. The rest of this paper is organized as follows. Section II gives an overview of the luminescence-based sensing method. Section III describes the system architecture in detail. Section IV demonstrates the measurement results from the benchtop experiments and a human subject test. Section V compares the performance of our design with the existing $PtcCO_2$ monitors. Finally, Section VI concludes this paper.

## II. Luminescence Sensing

$CO_2$-sensitive luminescent materials have found application in continuous $CO_2$ monitoring in diverse fields such as clinical [21], [26], environmental [27], [28], and oceanographic [29] applications. These materials emit light when illuminated by a specific-wavelength light source. The illumination excites the atomic groups, named luminophores in the luminescent material, to a higher energy state from the ground state. The luminophores transiting back to the ground state emit photons that produce a light emission called luminescence [30]. The collision of $CO_2$ molecules with the luminophores during this transition changes the intensity and lifetime of luminescence. In this work, we present a miniaturized $PtcCO_2$ monitor which quantifies $CO_2$ based on the luminescence characteristics of a commercial $CO_2$-sensitive film ($CO_2$ Sensor Spot CD1T, PreSens Precision Sensing GmbH). The sensing film incorporates two luminophores which have distinct luminescence properties. The resulting duality enables a third approach to sense $CO_2$ changes by a method called time-domain dual lifetime referencing (t-DLR), in addition to monitoring luminescence intensity and lifetime.

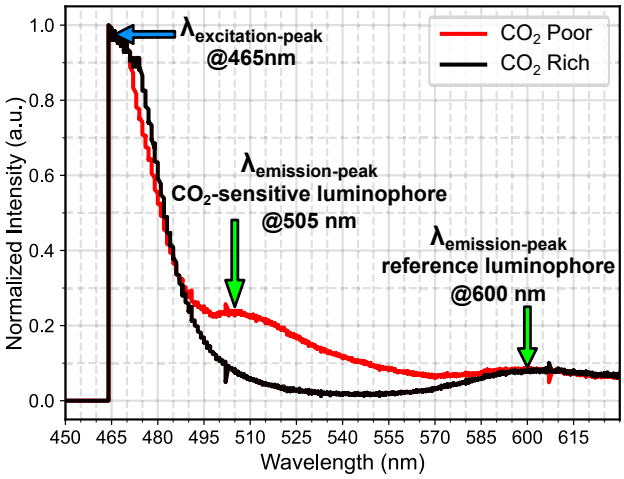


Fig. 2. The emission spectra of the sensing film when it is exposed to blue light excitation at 465 nm, under $CO_2$-poor and $CO_2$-rich conditions [25].

### A. Luminescence Intensity

The $CO_2$-sensitive film, which we will refer to as the sensing film in the rest of the paper, emits light in two different peak wavelengths in response to a blue light excitation ($\lambda_{peak}$ = 465 nm), as demonstrated in Fig.2. The first emission peak in the sensing film occurs at 505 nm, produced by the luminescence of the $CO_2$-sensitive luminophores, while the reference luminophores reach the peak luminescence at 600 nm. When $CO_2$ is introduced into the sensing film, the intensity of the luminescence from $CO_2$-sensitive luminophores decreases; however, the intensity of luminescence from the reference luminophores remains unaffected by the change in $CO_2$. Therefore, the total luminescence is proportional to the partial pressure of $CO_2$; hence, it can be used to measure $CO_2$. However, various confounding factors such as the photo-bleaching of the sensing film, variations in the photo-sensitivity of the luminescence detector, and variations in the intensity of the excitation source can impact the intensity measurements and thus affect the measurement accuracy [25].

### B. Luminescence Lifetime

Luminescence lifetime is described as the average time it takes for luminophores to return to the ground state upon excitation [30]. The lifetime of the $CO_2$-sensitive luminophores decreases with increasing $PCO_2$. Luminescence lifetime measurement is advantageous over intensity measurement as it is insensitive to changes in the photosensitivity of the luminescence detector or the strength of the excitation source [31], [32]. Despite this advantage, lifetime measurement for $CO_2$ monitoring is not practical due to the nanosecond (ns) range lifetime of $CO_2$-sensitive luminophores [30], [33]. Special optical instrumentation and high-speed electronics required for ns lifetime measurement make the design of a low-power and miniaturized measurement device challenging [34].

### C. Time-Domain Dual Lifetime Referencing

Relying on the fact that the measured luminescence intensity of both reference and $CO_2$-sensitive components are equally

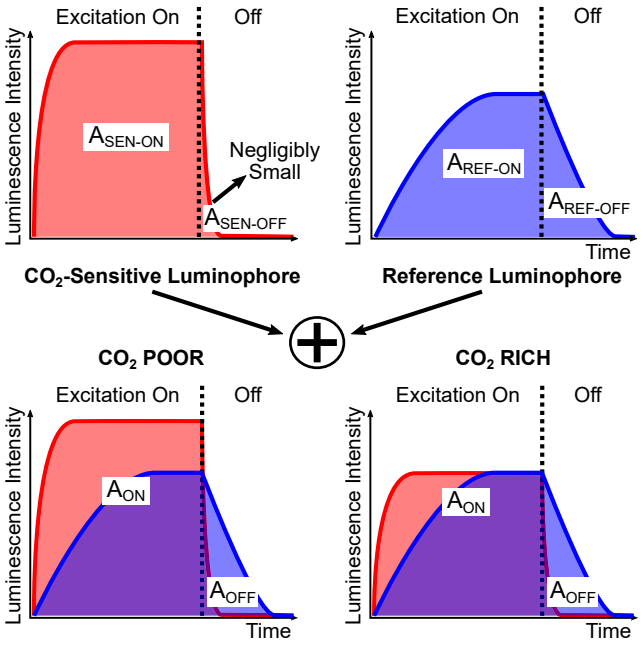


Fig. 3. The luminescence curves of the $CO_2$-sensitive, reference, and total luminophores in response to a pulsed illumination.

affected by confounding factors, such as the changes in excitation source strength or luminescence detector's photosensitivity, a ratio-metric method is proposed [35]. The core concept behind the ratio-metric method, called time domain dual lifetime referencing, is to produce a measurement outcome that is immune to external factors affecting both the luminescent materials. The time domain dual lifetime referencing method is explained through the following analysis. Initially, we depict the impact of the external factors using a variable $c_{EXT}$. Then, we develop the following equations to describe the luminescence of the $CO_2$-sensitive, $L_{SEN}$, and reference, $L_{REF}$, luminophores as:

$$L_{SEN} = \frac{c_{EXT}}{PCO_2} L_{SEN_0}, \tag{1}$$

$$L_{REF} = c_{EXT} L_{REF_0}, \tag{2}$$

where $L_{SEN_0}$ and $L_{REF_0}$ denote the luminescence constants of $CO_2$-sensitive and reference luminophores, respectively. The ratio of the luminescences, $L_{SEN}/L_{REF}$, becomes insensitive to the changes in external factors, as $c_{EXT}$ is canceled out. Nevertheless, capturing $L_{SEN}$ and $L_{REF}$ separately necessitates the use of two luminescence detectors with distinct spectral ranges and two signal pathways to process the luminescence data. Any mismatch in the signal pathway can result in a decrease in the measurement accuracy.

Fig.3 illustrates the luminescence intensity of each component as a function of time when the sensing film is excited with a pulse of blue light. Total luminescences during the excitation are the areas under the luminescence curves of $CO_2$-sensitive, $A_{SEN-ON}$, and the reference, $A_{REF-ON}$, luminophores, and they can be expressed as:

$$A_{SEN-ON} = \frac{c_{EXT}}{PCO_2} L_{SEN_0} \int_t L_{SEN-ON}(t), \tag{3}$$

$$A_{REF-ON} = c_{EXT} L_{REF_0} \int_t L_{REF-ON}(t), \tag{4}$$

where $L_{SEN-ON}(t)$ and $L_{REF-ON}(t)$ describe the luminescence intensity of each luminophore, $CO_2$-sensitive and reference, respectively, as a function of time. Hence, the total luminescence of the sensing film, $A_{ON}$, is equal to $A_{SEN-ON}$+$A_{REF-ON}$.

$$A_{ON} = c_{EXT}\left(\frac{L_{SEN_0}}{PCO_2} \int_t L_{SEN-ON}(t) + L_{REF_0} \int_t L_{REF-ON}(t)\right). \tag{5}$$

When the excitation is turned off, luminescences of the luminophores decay at a rate proportional to the their lifetimes and the total luminescences of $CO_2$-sensitive, $A_{SEN-OFF}$, and the reference, $A_{REF-OFF}$, luminophores, are as follows,

$$A_{SEN-OFF} = \frac{c_{EXT}}{PCO_2} L_{SEN_0} \int_t L_{SEN-OFF}(t), \tag{6}$$

$$A_{REF-OFF} = c_{EXT} L_{REF_0} \int_t L_{REF-OFF}(t), \tag{7}$$

where $L_{SEN-OFF}(t)$ and $L_{REF-OFF}(t)$ are designating the luminescence functions of the luminophores after the excitation. Since the lifetime of the $CO_2$-sensitive luminophore is in the ns range, the luminesce function decays rapidly. On the contrary, the lifetime of the reference luminophore is in the microseconds ($\mu$s) range, orders of magnitude longer than that of the $CO_2$-sensitive luminophore. Therefore, $A_{SEN-OFF}$ is negligible compared to $A_{REF-OFF}$. The total luminescence of the sensing film after the excitation, $A_{OFF}$, can simply be defined as $A_{REF-OFF}$, through the following equation:

$$A_{OFF} = c_{EXT} L_{REF_0}\left(\int_t L_{REF-OFF}(t)\right). \tag{8}$$

$A_{ON}$ depends on the luminescences of both luminophores, $c_{EXT}$, and $PCO_2$, while $A_{OFF}$ is determined by the luminescence of only the reference luminophore and $c_{EXT}$. By taking the ratio, $A_{ON}/A_{OFF}$, which we refer to as the luminescence ratio (LR), we obtain a measurement of $CO_2$ that is independent of the confounding factors, including excitation source strength and detector's photo-sensitivity, since the term $c_{EXT}$ is canceled out. This method allows for the necessary luminescence information to be captured and processed with a single detector and signal pathway, without the need for specialized optical instrumentation and high-speed electronics.

## III. System Architecture

The system architecture of the Ptc$CO_2$ monitoring prototype is demonstrated in Fig.4. The system is comprised of five main blocks: 1) an optical interface that incorporates a light-emiting diode (LED) to excite the sensing film, a photodiode (PD) to capture the resulting luminescence, and a $CO_2$-sensitive luminescence film to read $CO_2$ changes, 2) an LED driver for controlling the LED, 3) a transimpedance amplifier (TIA) for amplifying small photodiode currents, 4) a microcontroller

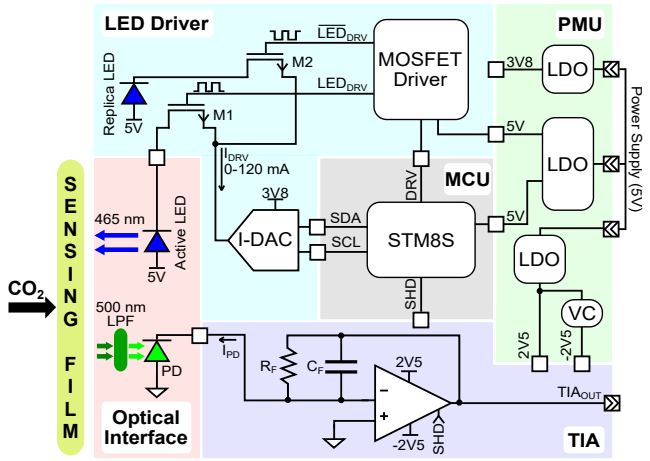


Fig. 4. System architecture of the PtcCO$_2$ monitoring prototype.

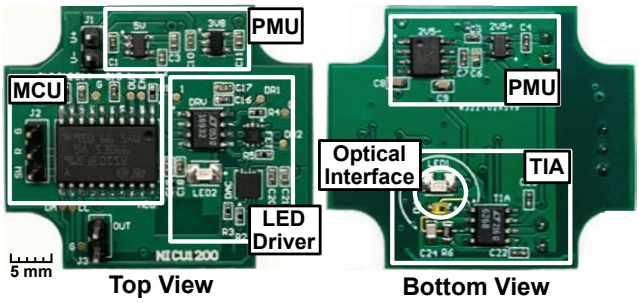


Fig. 5. PCB of the wearable PtcCO$_2$ monitor.

(MCU) for managing the control signals of the LED driver and the TIA blocks, 5) a power management unit that distributes power to the rest of the architecture from a single supply source. We implemented the prototype on a 37 mm×32 mm printed circuit board (PCB) shown in Fig.5. The real-time processing of the luminescence data and the calculations of the t-DLR method are performed off the board.

### A. Optical Interface

The optical interface consists of an LED (CLM1B, Cree) emitting blue light with a peak wavelength of 465 nm and a green-sensitive PD (SD019, Advanced Photonix) with a 500 nm long-pass filter (LPF) (Edmund Optics) placed on PD's photosensitive surface. The LPF passes the luminescence of the luminophores with peak wavelengths of 505 nm and 600 nm, while blocking the stray light from the LED. The optical interface is deployed on the bottom layer of the PCB, which faces the user's skin.

### B. LED Driver

The LED driver incorporates a current-sinking digital-to-analog converter (I-DAC) (AD5398, Analog Devices), a high-speed dual N-channel MOSFET driver (LTC1693, Analog Devices), two N-channel power MOSFETs (M1 and M2) (CSD85301Q2, Texas Instruments), and a replica LED. The purpose of the LED driver is to generate excitation pulses with adjustable frequency, pulse width, and drive strength. The LED driver has an inverting ($\overline{LED}_{DRV}$) and a non-inverting ($\text{LED}_{DRV}$) channel that take the drive signal (DRV) from the MCU, which controls the frequency and pulse width of the DRV signal. $\text{LED}_{DRV}$ and $\overline{LED}_{DRV}$ drive the gates of M1 and M2, respectively. M1 manages the active LED in the optical interface, while the replica LED is controlled by M2.

The replica LED ensures that the driver operates continuously without switching off, so all the internal nodes of the current source are set before the active LED turns on. This operation scheme is required to generate sharp and narrow excitation pulses down to several microseconds by overcoming the slow transients of the I-DAC, such as slow output current settling time (several hundreds of microseconds) and slew rate of the N-channel driver (0.3 mA/$\mu$s). The I-DAC, which has 120 mA output current capability with 10-bit resolution (117 $\mu$A/LSB), sets the current of the driver. The MCU adjusts the output current of the I-DAC via a 2-wire serial interface: serial data (SDA) and serial clock (SCL). A programmable current for the LED driver provides the ability to control the drive current, $\text{I}_{DRV}$, with various excitation intensities.

### C. Transimpedance Amplifier

The TIA amplifies the photocurrent of PD, $\text{I}_{PD}$, resulting from the luminescence of the sensing film in response to the excitation pulse. The typical photosensitivity of the photodiode is 0.12 A/W, and the optical power of the LED is tens of microwatts depending on the excitation strength. Therefore, the input current of the TIA is around several microamperes. The feedback resistor, $\text{R}_F$, sets the transimpedance gain. We chose $\text{R}_F$ to be $\sim$ 250 k$\Omega$ to amplify the small input current up to several volts without saturating the TIA, operating on rail-to-rail $\pm$ 2.5 V. The value of $\text{R}_F$ affects another important parameter, the bandwidth of the TIA. The bandwidth must be high enough to capture the luminescence curve of the reference luminophores decay after the LED is turned off without distortion. The decay rate ($\tau$) is equal to the lifetime of the reference luminophores, which is in the $\mu$s regime. Given a $\tau$ of 1 $\mu$s, the bandwidth of the TIA should be greater than $\frac{1}{2\pi\tau} \approx$ 160 kHz. The bandwidth of the TIA, $\text{f}_{BW}$, is,

$$f_{BW} = \sqrt{\frac{GBW}{R_F(C_{IN} + C_F)2\pi}}, \tag{9}$$

where GBW is the gain-bandwidth product of the TIA, $\text{C}_{IN}$ is the total input capacitance at the inverting node, and $\text{C}_F$ is the feedback capacitance [36]. We chose a TIA with a high GBW (LTC6268, Analog Devices), 500 MHz. $\text{C}_{IN}$ is equal to the combination of the input capacitance of the TIA, 0.5 pF, and the junction capacitance of PD, 28 pF. Considering the capacitances of the pads, connecting PD with the inverting input of the TIA, $\text{C}_{IN}$ is estimated to be around 30 pF. If we assume $\text{C}_F$ is negligibly small compared to $\text{C}_{IN}$, and solve (9), we find the bandwidth to be approximately 3 MHz.

In the resistive-feedback TIA configuration, the total input capacitance, $\text{C}_{IN}$, and the feedback resistor, $\text{R}_F$, introduce a pole that can cause stability issues. Therefore, the feedback capacitance, $\text{C}_F$, is added in parallel to $\text{R}_F$ to stabilize the loop. We determine the value of $\text{C}_F$ by incorporating $\text{C}_{IN}$, $\text{R}_F$, and GBW of the TIA [36] in the following equation,

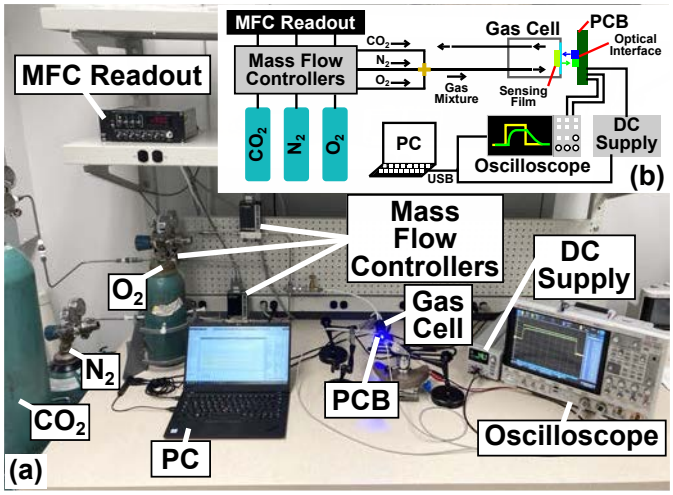


Fig. 6. (a) Picture and (b) illustration of the setup for gas chamber and benchtop experiments.

$$C_F > \sqrt{\frac{C_{IN}}{R_F GBW \pi}}. \tag{10}$$

Therefore, the minimum value for $C_F$ is around 0.3 pF. We select $C_F$ as 0.7 pF to guarantee a stable operation, accounting for the stray capacitance of the board that can increase $C_{IN}$. The TIA can operate in the shutdown mode between excitation pulses to save power. In this mode, the TIA consumes as low as 1 mA current. The MCU generates the shutdown signal, SHD, to control the operation of the TIA.

### D. Microcontroller

The MCU (STM8S103F3, STMicroelectronics) generates DRV, SDA, SCL, and SHD control signals. We utilize a general-purpose timer to create the DRV excitation pulses. The 2-wire serial interface in I-DAC is established with an inter-integrated circuit ($I^2C$) protocol managed by the MCU. SHD signal is created using a general-purpose output port. We program the MCU via a single wire interface module (SWIM).

### E. Power Management Unit

The PMU consists of a 5 V-fixed output low dropout (LDO) regulator (TPS73250, Texas Instruments) to supply power to the MCU and the LED driver, a 2.5 V-fixed output LDO regulator (TPS73225, Texas Instruments), and a switched capacitor voltage converter (VC) (LM2660, Texas Instruments) to generate $\pm$2.5 V for the TIA, a 3.8 V-fixed output LDO regulator (TPS763, Texas Instruments) to power-up the I-DAC. A single 5 V supply powers the PMU.

## IV. Measurement Results

This section showcases the measurement results evaluating the various aspects of the proposed prototype. Our experimentation began by determining the minimum pulse width to excite a sufficient amount of luminophores for optimal power consumption. Subsequently, we measured the critical design metrics, including power consumption and bandwidth.

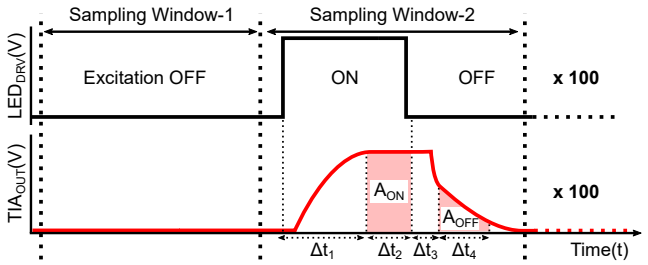


Fig. 7. Sampling windows of the signals $\text{LED}_{DRV}$ and $\text{TIA}_{OUT}$. The data acquisition is managed by a MATLAB script which controls the oscilloscope.

Following that, we proceeded with the gas experiments in which we examined the $PCO_2$ monitoring performance of our prototype and assessed the impact of excitation intensity variation. Next, we examined how various confounding factors and measurement drift affect the performance of the sensing film. Finally, we tested our prototype on a human subject.

### A. Measurement Setup

The benchtop setup, demonstrated in Fig.6, consists of three gas cylinders containing $CO_2$, nitrogen ($N_2$), and oxygen ($O_2$). A mass flow controller (MFC) regulates the flow rate of each gas cylinder via an MFC readout (247C, MKS Instruments). The gas mixture flows through a small gas cell (30 $cm^3$) where the sensing film is placed. The ratio of the $CO_2$'s flow rate to the gas mixture's flow rate determines $PCO_2$ in the gas cell based on the ideal gas law. We covered the gas cell with an opaque material to minimize the exposure to the ambient light, leaving a small opening for the PCB to interface with the sensing film.

The prototype's output, $\text{TIA}_{OUT}$, and the excitation signal, $\text{LED}_{DRV}$, are fed into an oscilloscope (MSOX6004A, Keysight). A personal computer (PC) controls the supply and the oscilloscope via a universal serial bus (USB). A MATLAB script running on the computer manages the oscilloscope for data acquisition and applies the t-DLR method. Fig.7 depicts the timing of $\text{LED}_{DRV}$ and $\text{TIA}_{OUT}$ fed into this script. The oscilloscope acquires the first sampling window when $\text{LED}_{DRV}$ is OFF. The second sampling window with the same duration captures $\text{TIA}_{OUT}$ right before, during, and after the excitation. This sequence repeats itself consecutively 100 times, averaging the samples of $\text{TIA}_{OUT}$ for the first and second windows to minimize the measurement noise. The average of the first and second windows, $\overline{TIA}_{OUT1}$ and $\overline{TIA}_{OUT2}$, represent the output of the TIA due to the ambient light and luminescence, respectively. $\overline{TIA}_{OUT1}$ is subtracted from $\overline{TIA}_{OUT2}$ to produce $\overline{TIA}_{OUT}$, which is cleared from the effect of the ambient light.

The MATLAB script calculates the LR from $\overline{TIA}_{OUT}$. First, the script detects the instances where the excitation is turned ON and OFF from the rising and falling edges of $\text{LED}_{DRV}$. Once a rising edge is detected, the script waits for a duration of $\Delta t_1$ before integrating $\overline{TIA}_{OUT}$. $\Delta t_1$ considers the delay between $\text{LED}_{DRV}$ and $\text{TIA}_{OUT}$ and the time it takes the luminescence response to settle. Following this duration, $\text{TIA}_{OUT}$ is integrated for a duration of $\Delta t_2$ until a falling edge is detected to calculate $A_{OFF}$. Then, the script waits for

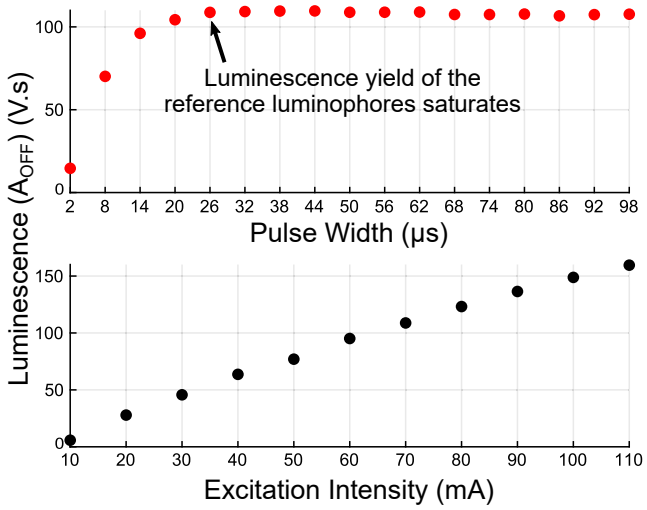


Fig. 8. Average luminescence of the reference luminophores ($A_{OFF}$) for a varying excitation pulse width and intensity at $PCO_2$ = 76 mmHg.

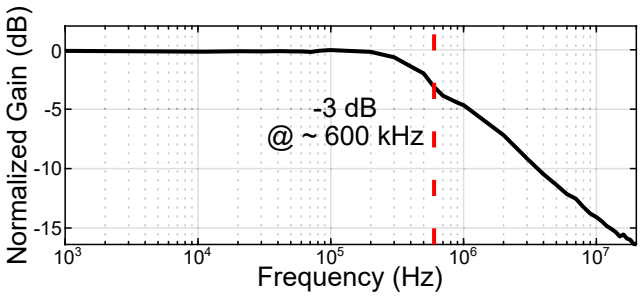


Fig. 9. Measured magnitude response of the transimpedance amplifier.


Fig. 10. Breakdown of the average power consumption.

a duration of $\Delta t_3$ before integrating $\overline{TIA}_{OUT}$ again. $\Delta t_3$ considers the delay between $LED_{DRV}$ and $TIA_{OUT}$ and the decay time of the $CO_2$-sensitive luminophores. Although the lifetime of the $CO_2$-sensitive luminophores is a few nanoseconds, which is negligible compared to the lifetime of the reference luminophores, the decay of the $CO_2$-sensitive luminophores can stretch to several hundreds of nanoseconds due to the finite bandwidth of the TIA, influencing the early portion of the luminescence decay. After the $CO_2$-sensitive luminophores ultimately decay, $A_{OFF}$ is calculated by integrating $TIA_{OUT}$ for a duration of $\Delta t_4$ until the luminescence decays. We chose the length of the sampling windows based on the duration of the excitation pulse width and the decay time of the reference luminophores, which is about 3-5 $\mu$s, depending on the excitation intensity.

### B. Benchtop Experiments

*1) Optimal Excitation Pulse Width:* The output signal of our prototype, $TIA_{OUT}$, is a function of the sensing film's luminescence yield, which depends on the pulse width and intensity of the excitation signal. Increasing these parameters boosts the luminescence yield and consequently enhances the output signal quality. However, increasing the pulse width and excitation intensity also contributes to the power consumption; moreover, excessive excitation leads to photobleaching of the sensing film, degrading the measurement accuracy. Hence, it is imperative to determine the optimal values for the excitation to ensure optimal performance.

We assessed the excitation efficiency by monitoring the luminescence of the reference luminophores, $A_{OFF}$. The average luminescence of 100 samples of $A_{OFF}$ was measured with varying excitation pulse width and intensity, as demonstrated in Fig.8. We performed this experiment at 76 mmHg $PCO_2$, a high $CO_2$ level, to reduce the yield of $CO_2$-sensitive luminophores during the decaying portion of the luminescence. The pulse width is varied from 2 $\mu$s to 98 $\mu$s in steps of 6 $\mu$s at a fixed excitation intensity ($I_{DRV}$ = 70 mA). $A_{OFF}$ increases with the pulse width up to 26 $\mu$s and stays relatively constant beyond this point, indicating that 26 $\mu$s is the threshold pulse width for achieving maximum luminescence yield. We selected the optimal pulse width to be 32 $\mu$s, slightly higher than the measured threshold value, to maintain maximum yield in case of obtaining slightly different pulse width than expected during measurements.

We varied the excitation intensity by changing the LED drive current, $I_{DRV}$ from 10 mA to 110 mA when the pulse width was fixed at 32 $\mu$s. The relation of the excitation intensity is linear in the given range. The more we increase the intensity, the more integrated luminescence we observe; therefore, there is no optimum for the excitation intensity. We set the excitation intensity as 100 mA to obtain a relatively higher yield.

*2) Circuit Characterization:* The measured magnitude response of the transimpedance amplifier in the frequency domain is depicted in Fig.9. To measure the magnitude response, we connected a signal generator parallel to the PD. First, we set the output impedance of the signal generator to ~250 kΩ, equal to the feedback resistance of the TIA, $R_F$, to achieve unity gain. Next, we fed a sinusoidal wave with 1 $V_{pp}$ amplitude and -0.5 V DC offset. With the given output impedance, this input injects a ~4 $\mu A_{pp}$ current into the inverting input of the TIA. We covered the photo-sensitive area of the PD with black tape to avoid photocurrent. Then, we swept the frequency of the input signal from 1 kHz to 20 MHz and recorded $TIA_{OUT}$. The normalized magnitude response is obtained by dividing $TIA_{OUT}$ by the output of the signal generator. According to this measurement, the bandwidth of the TIA is measured as 600 kHz.

A breakdown of the prototype's average power consumption is demonstrated in Fig.10. The LED driver consumes 25.6 mW, significantly more than any other block. The active LED excites the sensing film for 32 $\mu$s every 1 ms. The TIA is enabled during the sampling windows 1 and 2, illustrated in Fig. 7, and shut down otherwise. The other blocks operate continuously in this 1 ms interval. The system collects 100 samples for averaging in 0.1 s and turns off all the blocks for ~25 s. This sequence repeats continuously generating one

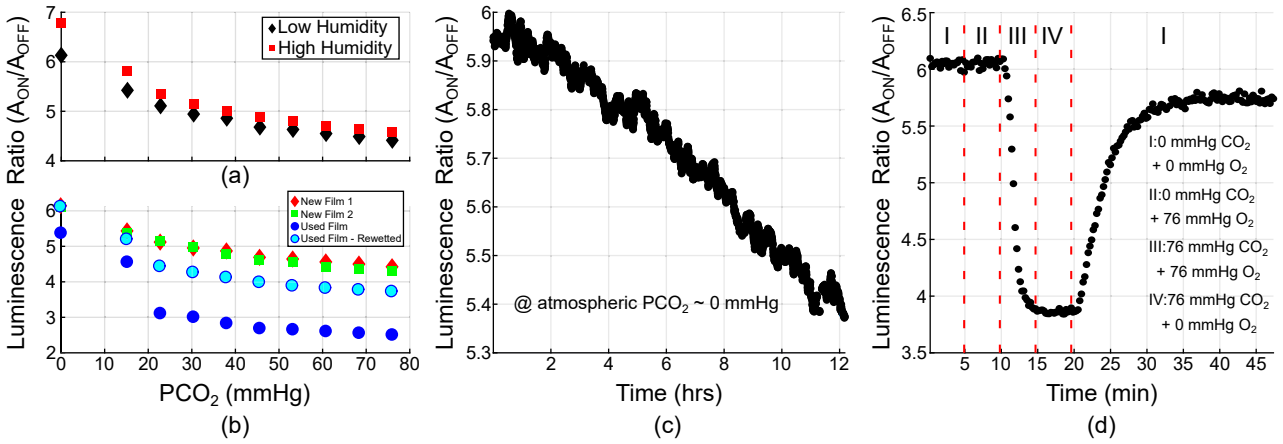


Fig. 11. Benchtop experiment results presenting the effects of (a) humidity, (b) part-to-part variation, (c) measurement drift, and (d) oxygen presence on the LR.

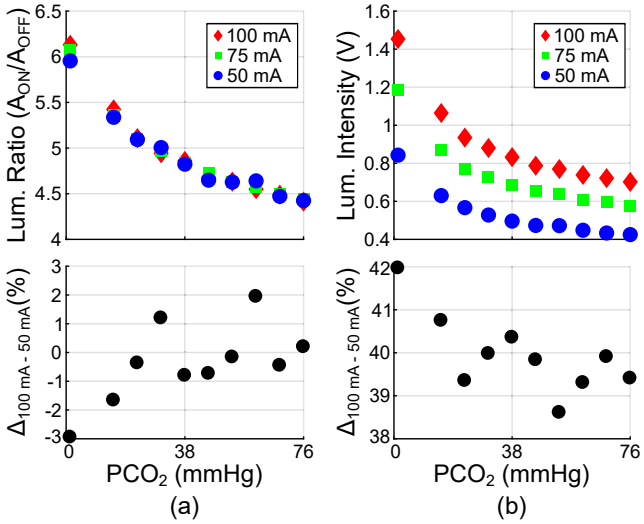


Fig. 12. (a) Luminescence (Lum.) ratio, and (b) intensity measured by the prototype for varying LED drive current, $I_{DRV}$, in 0-76 mmHg $PCO_2$ range.

LR measurement every 25 s. With this operating scheme, the prototype consumes 30.1 mW on average.

### C. Gas Chamber Experiments

The $PtcCO_2$ of healthy humans changes between 35-45 mmHg; however, the values can fluctuate outside this range for people with respiratory disorders [37]. Therefore, a $PtcCO_2$ monitor must be capable of quantifying $CO_2$ in a broader range. We studied the monitoring performance of our prototype on the test bench with varying $CO_2$ levels. We incrementally increased the $PCO_2$ of the gas cell, where the sensing film is located, from 0 to 76 mmHg. Fig.12.a illustrates the relationship between the LR and $PCO_2$ for three distinct LED drive currents, 50 mA, 75 mA, and 100 mA, as well as the percentage variation between 50 mA and 100 mA ($\Delta_{100mA-50mA}\%$). The results not only prove that the prototype can quantify $CO_2$ in a clinically relevant range but also demonstrates the robustness of the readings against the changes in the excitation intensity thanks to the ratiometric approach. While reducing the excitation intensity by half introduces an average of 40% change in the luminescence intensity readings, as shown in Fig.12.b, the percentage change in the LR is, at most, only 3%.

*1) Sensing Film Characterization:* We performed several characterization experiments on the $CO_2$-sensitive luminescent film to investigate the film's performance in various conditions. With the gained knowledge, potential correction mechanisms can be incorporated into future versions of luminescent film-based $PtCO_2$ monitors. We measured the LR for $PCO_2$ ranging from 0 to 76 mmHg at a low (30%) and high (100%) humidity conditions. Fig.11.a shows the effect of humidity on the LR. The increased humidity adds an offset to readings which affects the measurement accuracy. Nevertheless, the offset is almost constant within 23-76 mmHg and can be compensated by adding a humidity sensor to the monitor, output of which can be used to correct the readings. Alternatively, the sensing film can be contained in a hydrophobic coating to avoid the interference of skin humidity [38].

Measurement drift is another critical factor affecting the monitor's performance during long-term continuous monitoring. According to Food and Drug Administration's guidance on $PtcCO_2$ monitors, the drift in the $PtCO_2$ reading should not exceed 10% of the initial reading over the calibration period defined for the monitor [39]. Fig.11.c demonstrates the drift in the measured LR over 12 hours at atmospheric $PCO_2$ ($\sim$ 0 mmHg) and constant temperature (25°C). The initial $PtcCO_2$ reading drifts by 10% in $\sim$12 hours, indicating that the monitor needs to be calibrated every 12 hours, equivalent to the calibration interval of the clinical benchtop $PtcCO_2$ monitors [16].

In order to evaluate the variability of the sensing film across different parts, we conducted tests by examining the correlation between the LR and $PCO_2$, as illustrated in Fig.11.b. We used two new films as well as a sensing film that underwent continuous measurement for 12 hours. The average absolute % variation between the readings of the new films was found to be 1.7%. At 0 mmHg, the LR of the used film is $\sim$10% lower than that of the new films due to the measurement drift that occurred in 12 hours. In the presence of $CO_2$, more evidently in the 23-76 mmHg $PCO_2$ range, the LR of the used sensing film is significantly lower, $\sim$40% less than the readings of the new films. We believe the prolonged use of the sensing

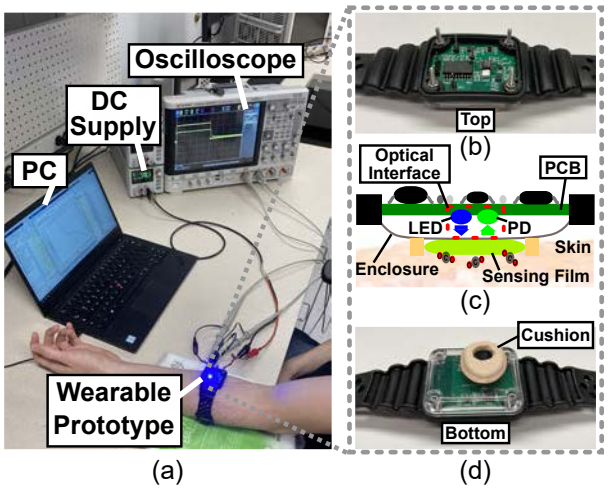


Fig. 13. Illustrations of (a) the human subject test setup, (b) top view of the wearable $PtcCO_2$ monitor, (c) illustration of the wearable $PtcCO_2$ monitor, (d) bottom view of the wearable $PtcCO_2$ monitor.

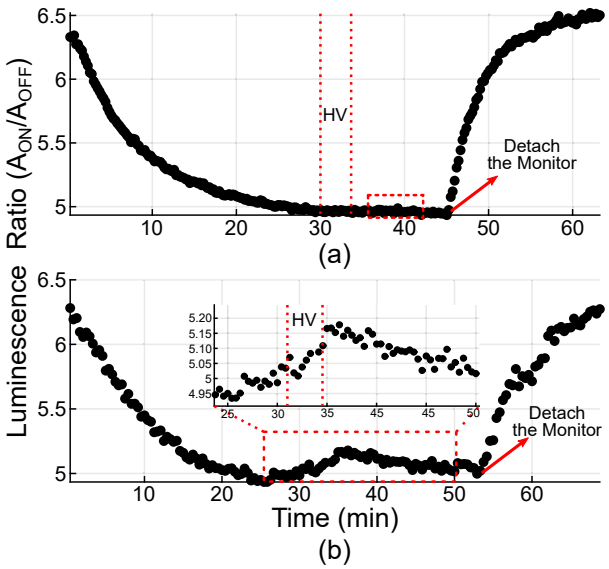


Fig. 14. Measured LR on the (a) forearm and (b) fingertip during 3.5 minutes hyperventilation (HV).

film causes the sensing layer in the film to dry out, decreasing the luminescence yield. The sensing layer needs to be rewetted regularly to prevent sensing layer from drying. After rewetting the used film, the LR of the used film recovers back to 10 % below the readings of the new films, as demonstrated in Fig.11.b.

In addition, we examined the sensing film's cross-sensitivity to oxygen, given that the diffusion of oxygen molecules through the skin is a well-established phenomenon that has been researched in the field of transcutaneous sensing [31], [40]. Results depicted in Fig.11.d prove that variations in partial pressure of $O_2$ ($PO_2$) do not affect the LR, which suggests that the sensing film employed in this study is not responsive to $O_2$.

### *D. Human Subject Experiments*

To assess the effectiveness of our prototype on skin, we conducted a test on human subjects, shown in Fig.13.a. The PCB is embedded in a wristband enclosure (BW2, Serpac) to form a wearable prototype as shown in Fig. 13.b and 13.d, which show the top and bottom views, respectively. The optical interface is situated inside the enclosure on the bottom side of the wearable as illustrated in Fig.13.c. The sensing film is affixed to the surface of the enclosure, aligned with the optical interface, and surrounded by a cushion to create comfortable contact with the skin. The top side of the wearable, demonstrated in Fig.13.b, remains open to accommodate the oscilloscope probe and power connections.

To begin with, we positioned the wearable prototype on the subject's forearm. Fig.14.a demonstrates the measured LR right after the prototype was placed on the forearm. In 30 minutes, the readings stabilize around a LR value that is 6.4 starting from a value corresponding to atmospheric $PCO_2$. Once the readings had stabilized, the subject hyperventilated for 3.5 minutes to induce a change in $PtcCO_2$. However, we were unable to observe any changes other than an insignificant increase in the LR, several minutes after the hyperventilation. We waited for 10 minutes after the hyperventilation and then removed the prototype from the subject's forearm.

Despite our inability to detect changes induced by hyperventilation, we were able to effectively observe significant changes in $PtcCO_2$ during the transition from atmospheric $PCO_2$ to the skin $PtcCO_2$ value, both at the beginning and end of the measurement. It is worth noting that regulating $PaCO_2$ and $PtcCO_2$ in healthy individuals is more challenging compared to $PaO_2$ and partial pressure of transcutaneous $O_2$ ($PtcO_2$) due to their notably smaller range [41].

The available literature provides different rates and quantities of transcutaneous oxygen diffusion for various parts of the body [42]. It has been suggested that the settlement time is shorter and the diffusion of molecules is more significant in the fingers, making them one of the ideal sites for measurement [43]. In the next test, we placed the subject's index finger on the sensing film and measured the LR during hyperventilation. This time, we could detect the changes in the LR induced by hyperventilation. The increase in the LR indicated a decrease of approximately 5 mmHg in $PtcCO_2$, an outcome expected following hyperventilation.

Based on the results of the two experiments conducted on human subjects, it can be concluded that the first miniaturized prototype utilizing the t-DLR method possesses sufficient resolution to identify subtle changes in body sites with a higher $CO_2$ diffusion rate, but not the reverse. These measurement outcomes should be taken into account while determining the resolution specifications of the AFE for the subsequent version of the $PtcCO_2$ monitors.

## V. Benchmarking

Over the past few years, several research groups have focused on developing miniaturized and wearable transcutaneous monitors, including $PtcCO_2$ and $PtcO_2$ monitors. To assess the performance of our prototype, we compared its performance with the recent work in the literature in Table.I. According

TABLE I
COMPARISON OF PERFORMANCE PARAMETERS OF TRANSCUTANEOUS MONITORS

| Parameters | [19] 2020 | [20] 2021 | [18] 2021 | [21] 2022 | [44] 2023 | **This Work** 2023 |
|---|---|---|---|---|---|---|
| Publisher | IEEE EMBC | IEEE BioCAS | IEEE Sensors | MPDPI Biosensors | IEEE TBioCAS | IEEE TBioCAS |
| Monitor Type | $PtcCO_2$ | $PtcCO_2$ | $PtcCO_2$ | $PtcCO_2$ | $PtcO_2$ | $PtcCO_2$ |
| Sensing Principle | Infrared | Intensity | Infrared | Intensity | Lifetime | t-DLR |
| Wearable Form | Wristband | NA | Wristband | Wristband | NA | Wristband |
| PCB Size(mm×mm) | NA | 60.0×55.0 | ⌀20.9×18.1* | NA | 100×50 | 37×32 |
| Supply Voltage (V) | NA | 5.0 | 3.3 | NA | 3.0 | 5.0 |
| Power Consumption (mW) | NA | 64.3 | 3.4 | NA | 9.9 | 30.1 |
| Transimpedance Gain | NR | 1 MΩ | NR | NA | 12.5 kΩ – 200 kΩ | 250 kΩ |
| Bandwidth (Hz) | NR | 1 M | NR | NA | NA | 600 k |
| Range (mmHg) | 30 – 50 | 0 – 75 | 0 – 38 | 0–50 | 0–418† | 0–76 |

**Note:** * dimensions of the sensor head only.NA - not addressed.NR - not relevant.†The range of $PtcO_2$ in humans is greater than that of $PtcCO_2$.

to our literature review, our prototype is the first $PtcCO_2$ monitor that utilizes t-DLR as the sensing principle. [19] and [18] are nondispersive infrared (NDIR)-based $PtcCO_2$ monitors, while [20] and [21] rely on sensing the luminescence intensity of a $CO_2$-sensitive film for monitoring. [44] is a luminescence lifetime-based $PtcO_2$ sensor. Our prototype has the smallest reported PCB size, 37 mm×32 mm, making it suitable for use in a small wristband wearable. The high transimpedance gain of our prototype enables us to detect small changes in luminescence and changes in $PCO_2$ with a resolution as small as 5 mmHg within the 0-76 mmHg range, which is the range most relevant for medical diagnosis and treatment. Nevertheless, the human subject tests indicate that the resolution should be enhanced to detect smaller changes, even as low as 1 mmHg in $PtcCO_2$, at measurement sites where the $CO_2$ diffusion is slower due to physiological factors.

The prototype has an average power consumption of 30.1 mW, with the LED driver being the main contributor due to the replica LED that dissipates most of the power to maintain a constant current source to meet the I-DAC's settling requirements. To assess the board under varying LED drive currents, we utilized the I-DAC, which allowed us to determine the drive current. As we determined the drive current in this work, the LED driver topology can be simplified to a common source configuration without the replica LED and I-DAC in a future prototype. Without the replica LED, the prototype consumes $\sim$ 6.1 mW. In [18], a low-power commercial NDIR $CO_2$ sensor, which consumes 3.4 mW, without custom-designed electronics. [44] employs a low-power multimodal sensor front-end that both drives the LED and processes the luminescence information, resulting in reduced power consumption.

## VI. CONCLUSION

In this paper, we have introduced a t-DLR-based wearable monitor for measuring $PtcCO_2$. The benchtop experiments have proved that our monitor is capable of detecting changes in $PCO_2$ within the clinically significant range of 0-76 mmHg. We demonstrated that the LR produced by the t-DLR method is far less vulnerable to changes in the excitation intensity compared to the luminescence intensity. Within the 0-76 mmHg $PCO_2$ range, a 50% change in the excitation intensity caused a maximum variation of 3% in the LR, whereas the average change in the luminescence intensity was 40%. We analyzed the impact of several confounding factors on the sensing film's behavior, such as skin humidity and $PtcO_2$. We further characterized the sensing film by investigating the changes in its luminescence properties after prolonged use. The designed $PtcCO_2$ monitoring prototype fits into a small wristband wearable and consumes 30.1 mW of power. Finally, we conducted a trial on a human subject using our prototype to assess its effectiveness in monitoring $PtcCO_2$ in a real-life scenario. We identified hyperventilation from the fingertip measurements, proving the concept of first-of-its-kind t-DLR-based $PtcCO_2$ monitoring on a human subject.

## REFERENCES


[1] "Chronic obstructive pulmonary disease (copd)." [Online]. Available: https://www.who.int/news-room/fact-sheets/detail/chronic-obstructive-pulmonary-disease-(copd)

[2] W. W. Labaki and M. K. Han, "Chronic respiratory diseases: a global view," *The Lancet Respiratory Medicine*, vol. 8, no. 6, pp. 531–533, 2020.

[3] D. Sankaran *et al.*, "Non-invasive carbon dioxide monitoring in neonates: methods, benefits, and pitfalls," *Journal of Perinatology*, pp. 1–10, Jun. 2021.

[4] U. Guler *et al.*, "Sensors for Neonatal Monitoring," in *Reference Module in Biomedical Sciences*. Elsevier, Jan. 2022.

[5] I. M. Costanzo *et al.*, "Respiratory Monitoring: Current State of the Art and Future Roads," *IEEE Reviews in Biomedical Engineering*, pp. 1–1, 2020, conference Name: IEEE Reviews in Biomedical Engineering.

[6] "Severinghaus blood gas analyzer," Jan 2021. [Online]. Available: https://www.woodlibrarymuseum.org/museum/severinghaus-blood-gas-analyzer/

[7] "Tcm tosca monitor." [Online]. Available: https://www.radiometeramerica.com/en-us/products/transcutaneous-monitoring/tcm-tosca

[8] "Transcutaneous co2 monitoring (tcm)," Aug 2022. [Online]. Available: https://www.sentec.com/transcutaneous-monitoring/

[9] W. van Weteringen *et al.*, "Validation of a New Transcutaneous $tcPO_2$/$tcPCO_2$ Sensor with an Optical Oxygen Measurement in Preterm Neonates," *Neonatology*, vol. 117, no. 5, pp. 628–636, 2020.

[10] J. Carrington *et al.*, "Transcutaneous carbon dioxide monitoring could reduce physical contact with COVID-19 patients," *American Journal of Hospital Medicine*, Sep. 2021.

[11] M. Dicembrino *et al.*, "End-tidal CO2 and transcutaneous CO2: Are we ready to replace arterial CO2 in awake children?" *Pediatric Pulmonology*, vol. 56, no. 2, pp. 486–494, 2021.

[12] B. S. Nassar and G. A. Schmidt, "Estimating Arterial Partial Pressure of Carbon Dioxide in Ventilated Patients: How Valid Are Surrogate Measures?" *Annals of the American Thoracic Society*, vol. 14, no. 6, pp. 1005–1014, Jun. 2017.

[13] K. P. Sullivan *et al.*, "Transcutaneous carbon dioxide pattern and trend over time in preterm infants," *Pediatric Research*, pp. 1–7, Jan. 2021.

[14] J. W. Severinghaus and A. Freeman, "Electrodes for Blood PO, and pC0, Determination," p. 6, 1958.

[15] P. Eberhard, "The Design, Use, and Results of Transcutaneous Carbon Dioxide Analysis: Current and Future Directions," *Anesthesia & Analgesia*, vol. 105, no. 6, pp. S48–S52, Dec. 2007.

[16] W. van Weteringen *et al.*, "Novel transcutaneous sensor combining optical tcPO2 and electrochemical tcPCO2 monitoring with reflectance pulse oximetry," *Medical & Biological Engineering & Computing*, Nov. 2019.

[17] T. B. Tufan, D. Sen, and U. Guler, "An Infra-Red-Based Prototype for a Miniaturized Transcutaneous Carbon Dioxide Monitor," in *2021 43rd Annual International Conference of the IEEE Engineering in Medicine Biology Society (EMBC)*, Nov. 2021, pp. 7132–7135.

[18] V. V. Tipparaju *et al.*, "Wearable Transcutaneous CO2 Monitor Based on Miniaturized Nondispersive Infrared Sensor," *IEEE Sensors Journal*, pp. 1–1, 2021.

[19] P. Grangeat *et al.*, "Evaluation in Healthy Subjects of a Transcutaneous Carbon Dioxide Monitoring Wristband during Hypo and Hypercapnia Conditions*," in *2020 42nd Annual International Conference of the IEEE Engineering in Medicine Biology Society (EMBC)*, Jul. 2020, pp. 4640–4643.

[20] T. Tufan and U. Guler, "A Fluorescent Thin Film-Based Miniaturized Transcutaneous Carbon Dioxide Monitor," Oct. 2021.

[21] J. P. Cascales *et al.*, "A Patient-Ready Wearable Transcutaneous CO2 Sensor," *Biosensors*, vol. 12, no. 5, p. 333, May 2022.

[22] R. N. Dansby-Sparks *et al.*, "Fluorescent-Dye-Doped SolGel Sensor for Highly Sensitive Carbon Dioxide Gas Detection below Atmospheric Concentrations," *Analytical Chemistry*, vol. 82, no. 2, pp. 593–600, Jan. 2010.

[23] C.-S. Chu and J.-J. Syu, "Optical sensor for dual sensing of oxygen and carbon dioxide based on sensing films coated on filter paper," *Applied Optics*, vol. 56, no. 4, p. 1225, Feb. 2017.

[24] A. Mills and D. Yusufu, "Highly CO2 sensitive extruded fluorescent plastic indicator film based on HPTS," *Analyst*, vol. 141, no. 3, pp. 999–1008, Jan. 2016.

[25] T. B. Tufan and U. Guler, "A Miniaturized Transcutaneous Carbon Dioxide Monitor Based on Dual Lifetime Referencing," in *2022 IEEE Biomedical Circuits and Systems Conference (BioCAS)*, Oct. 2022, pp. 144–148.

[26] M. Čajlaković, A. Bizzarri, and V. Ribitsch, "Luminescence lifetime-based carbon dioxide optical sensor for clinical applications," *Analytica Chimica Acta*, vol. 573-574, pp. 57–64, Jul. 2006.

[27] X. Ge *et al.*, "A Low-Cost Fluorescent Sensor for pCO2 Measurements," *Chemosensors*, vol. 2, no. 2, pp. 108–120, Jun. 2014.

[28] C. Chu and M. Hsieh, "Optical carbon dioxide sensor based on the colorimetric change of -naphtholphthalein and internal reference fluorescent CIS/ZnS QDs," in *2017 25th Optical Fiber Sensors Conference (OFS)*, Apr. 2017, pp. 1–4.

[29] J. S. Clarke *et al.*, "Characterization of a Time-Domain Dual Lifetime Referencing pCO2 Optode and Deployment as a High-Resolution Underway Sensor across the High Latitude North Atlantic Ocean," *Frontiers in Marine Science*, vol. 4, 2017.

[30] J. R. Lakowicz, *Principles of fluorescence spectroscopy*, 3rd ed. New York: Springer, 2006.

[31] I. Costanzo *et al.*, "A Noninvasive Miniaturized Transcutaneous Oxygen Monitor," *IEEE Transactions on Biomedical Circuits and Systems*, vol. 15, no. 3, pp. 474–485, Jun. 2021.

[32] B. Kahraman *et al.*, "A Miniaturized Prototype for Continuous Noninvasive Transcutaneous Oxygen Monitoring," in *2022 IEEE Biomedical Circuits and Systems Conference (BioCAS)*, Oct. 2022, pp. 486–490, iSSN: 2163-4025.

[33] M. D. Marazuela, M. C. Moreno-Bondi, and G. Orellana, "Luminescence Lifetime Quenching of a Ruthenium(II) Polypyridyl Dye for Optical Sensing of Carbon Dioxide," *Applied Spectroscopy*, vol. 52, no. 10, pp. 1314–1320, Oct. 1998.

[34] L. Wei, Wenrong Yan, and D. Ho, "Recent Advances in Fluorescence Lifetime Analytical Microsystems: Contact Optics and CMOS Time-Resolved Electronics," *Sensors*, vol. 17, no. 12, p. 2800, Dec. 2017.

[35] I. Klimant *et al.*, "Dual Lifetime Referencing (DLR) — a New Scheme for Converting Fluorescence Intensity into a Frequency-Domain or Time-Domain Information," in *New Trends in Fluorescence Spectroscopy: Applications to Chemical and Life Sciences*, ser. Springer Series on Fluorescence, B. Valeur and J.-C. Brochon, Eds. Berlin, Heidelberg: Springer, 2001, pp. 257–274.

[36] *LTC6268 - 500MHz Ultra-Low Bias Current FET Input Op Amp*, Linear Technology, 2014.

[37] J. H. Storre *et al.*, "Transcutaneous monitoring as a replacement for arterial PCO(2) monitoring during nocturnal non-invasive ventilation," *Respiratory Medicine*, vol. 105, no. 1, pp. 143–150, Jan. 2011.

[38] E. J. Park *et al.*, "Hydrophobic Polydimethylsiloxane (PDMS) Coating of Mesoporous Silica and Its Use as a Preconcentrating Agent of Gas Analytes," *Langmuir*, vol. 30, no. 34, pp. 10 256–10 262, Sep. 2014, publisher: American Chemical Society.

[39] "Cutaneous Carbon Dioxide (PcCO2) and Oxygen (PcO2) Monitors - Class II Special Controls Guidance Document for Industry and FDA," Dec. 2002.

[40] I. Costanzo, D. Sen, and U. Guler, "A Prototype Towards a Transcutaneous Oxygen Sensing Wearable," in *2019 IEEE Biomedical Circuits and Systems Conference (BioCAS)*. Nara, Japan: IEEE, Oct. 2019, pp. 1–4.

[41] P. D. Wagner, "The physiological basis of pulmonary gas exchange: implications for clinical interpretation of arterial blood gases," *European Respiratory Journal*, vol. 45, no. 1, pp. 227–243, Jan. 2015. [Online]. Available: http://erj.ersjournals.com/lookup/doi/10.1183/09031936.00039214

[42] D. F. Blake, D. A. Young, and L. H. Brown, "Transcutaneous oximetry: variability in normal values for the upper and lower limb," *Diving and Hyperbaric Medicine*, vol. 48, no. 1, p. 2, Mar. 2018.

[43] L. Abigail et al., "Optimizing Transcutaneous Oxygen Measurement Sites on Humans," in *2023 45th Annual International Conference of the IEEE Engineering in Medicine Biology Society (EMBC)*, In Review.

[44] V. Vakhter et al., "A prototype wearable device for noninvasive monitoring of transcutaneous oxygen," *IEEE Transactions on Biomedical Circuits and Systems*, 2023.